IEEE Access
Multidisciplinary | Rapid Review | Open Access Journal

Received November 2, 2020, accepted November 28, 2020, date of publication December 4, 2020,
date of current version December 16, 2020.

Digital Object Identifier 10.1109/ACCESS.2020.3042541

Analysis and Design of a Single-Stage Bridgeless Isolated AC-DC Resonant Converter for Programmable AC Power Source Applications

ZHI ZHANG[1], JUNKAI WU[1], LIWEI MENG[1], ZHAOYUN ZHANG[1], (Senior Member, IEEE), XIAO TANG[1], BIHUA HU[2], AND WANG HU[3]

[1]Department of Electrical Engineering and Automation, Dongguan University of Technology, Dongguan 523808, China
[2]School of Automation and Electronic Information, Xiangtan University, Xiangtan 411105, China
[3]School of Electric Power Engineering, South China University of Technology, Guangzhou 510641, China

Corresponding author: Bihua Hu (ephubihua2015@mail.scut.edu.cn)

This work was supported in part by the Teaching Quality and Teaching Reform Project of Guangdong Province under Grant PX-3218216 and Grant 201801283006, and in part by the Dongguan Social Science and Technology Development Project under Grant 2019507140826 and Grant 2020507140141.

ABSTRACT This paper proposes a single-stage bridgeless isolated AC-DC power factor correction (PFC) topology, and this topology can realize the function of step-up and the galvanic isolation for the AC input and DC output voltages through single-stage power conversion process. Firstly, the operation principle of the topology is analyzed in details. Then, by reasonably designing the series resonant parameters, the zero-voltage-switching (ZVS) turn-on for the power switches in the primary-side and zero-current-switching (ZCS) turn-off for the output rectifier diodes in the secondary-side of the transformer can also be achieved under wide load range, and the voltage stress of the power switches are also reduced based on the active clamping technology. The design procedure for the key components of the proposed converter is also derived. Finally, a 3 kW experimental prototype based on SiC power devices with 85 kHz switching frequency is built to verify the correctness and feasibility of the proposed topology, and the experimental results show a good performance. It can operates in a wide input grid voltage range, 95.7% of peak conversion efficiency and 3.9% of total harmonic distortion(THD) value for grid current could be obtained.

INDEX TERMS AC-DC converter, power factor correction, series resonant, zero-voltage-switching, zero-current-switching.

I. INTRODUCTION

In order to reduce the harmonic pollution to the power grid and meet the harmonics regulations and standards of the international electrotechnical commission(IEC) and institute of electrical and electronics engineers(IEEE), active power factor correction(PFC) technique is widely adopted for many AC-DC converters, and these AC-DC equipments are widely used for uninterruptible power supply, communication power supply, electric vehicle on-board charger, programmable AC power source and others [1]–[3].

Isolated AC-DC PFC converters are becoming necessary for many industrial applications [4], [5]. The conventional isolated PFC topology has two stages, the first stage is implemented for rectifier and PFC functions, and the rear stage is designed for output voltage regulation and galvanic isolation [5]–[7]. Many combined topologies are proposed for different industrial applications in pursuit of high conversion efficiency and power density [8]–[10]. However, due to the separated topology structure of the front and rear stages, they have the disadvantages of high components count and complex control strategies, which would lead to high cost, large power losses and low conversion efficiency [5].

Single-stage isolated AC-DC PFC converters process the power conversion only in one stage, and they have the features of simple control structure, few components and high efficiency, their topological structure and control strategy become the research hotspot recently [11]–[16]. A single-stage single-switch isolated converter which combines the boost-like topology and forward topology is proposed in [11] for low voltage and low power application, it is suitable for wide range of line voltage applications with high factor

The associate editor coordinating the review of this manuscript and approving it for publication was Md. Rabiul Islam.

values, but it remains the low conversion efficiency and high grid current harmonic content. An improved single-stage boost-flyback with a synchronous rectifier is proposed in [12] for higher power factor and efficiency. A quasi-active PFC scheme is also presented in [13], the input inductor can operate in the discontinuous current mode (DCM), and the performance of lower harmonic content and high power factor could be achieved based on adding an auxiliary winding to the transformer of the cascade flyback stage. In addition, many new single-stage isolated topologies with soft-switching technique have been proposed for light-emitting diodes (LED) driver applications [14]–[16]. However, these single-stage isolated PFC topologies mentioned above are only suitable for low power applications [4], [17]–[20].

For high-power AC-DC application, a 1.6kW single-phase isolated Cuk PFC converter with digital double-loop control method is proposed in [21], and nearly unity power factor(PF), low THD of grid current and fast dynamic performance under load variation can be achieved, but only 91% of the conversion efficiency can be obtained due to the existence of input diode rectifier bridge and the hard switching operation state of the power devices. A novel bidirectional single-stage 1.5 kVA AC-DC converter for single-phase EV charging application is introduced in [22], it consists of a current-fed half-bridge converter on the primary side and a full-bridge converter on the secondary side of a high-frequency transformer, newly modulation method and control strategy are also presented to guarantee the soft switching condition for power switches in both direction of power flow, and almost 2.5% THD, up to 96.5% conversion efficiency can be achieved for full-load conditions. In [23], a 3 kW single-stage bridge-type AC-DC isolation converter with the current-fed full-bridge topology is proposed for high power PFC applications, zero-current-switching (ZCS) operation is realized for all power switches, but the THD value is over 5% at the rated power, and the input diode bridge still remains, the measured peak efficiency is around 93% to 94%. A combined phase-shift and frequency modulation for the 3.3 kW dual-active-bridge(DAB) AC-DC converter with PFC is presented in [24], it could realize the ZVS over the whole AC mains voltage period, the high power density, a wide output voltage range and a measured efficiency of 95% for 350V output voltage can be obtained, but the drawback of complex control strategy and utilization of two many power devices still remains. A 1.4kW single-stage AC-DC converter based on dual active bridge is proposed in [25], ZVS operation for the input-side power switches and ZCS operation for the output-side power switches can be achieved under certain load conditions, the maximum conversion efficiency can reach 96%. A 3.3kW bidirectional single-stage AC-DC converter by integrating the interleaved totem-pole PFC converter with the DAB is proposed in [26], the measured efficiency for both forward and reverse modes is almost identical with peak efficiencies of 96.7% and 96.2% respectively. But these topologies mentioned above use too many power switches, which will lead to high hardware costs.

In this paper, a novel single-stage AC-DC bridgeless isolated PFC for programmable AC power source application is presented as shown in Fig.1. ZVS of power switches on the primary side and ZCS of rectifier diodes on the secondary side of the high-frequency(HF) transformer can be achieved based on the resonant soft switching technique. It can operate with high input PF, wide range of input voltage and low THD value of grid current. Moreover, as the reduction of the input diode rectifier bridge and the soft-switching operation for power devices, the remarkable conversion efficiency of 95.7% can be achieved.

This paper is also organized as follows. The topology and operation principle of the proposed single-stage isolated AC-DC resonant converter are illustrated in section II. The details of the steady-state analysis and design consideration are also introduced in section III and IV respectively. In Section V, experimental results are shown to demonstrate the feasibility of the proposed single-stage topology based on a 3 kW prototype. Finally, the conclusion for this paper is contained in Section VI.

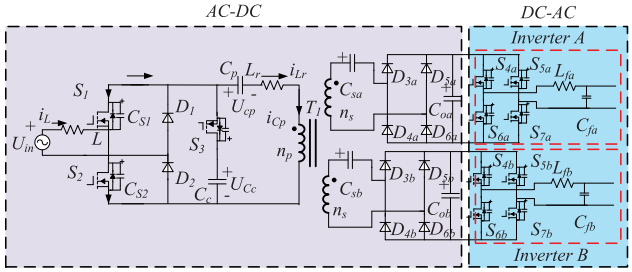

FIGURE 1. Topology of the programmable AC power supply.

II. PROPOSED SINGLE-STAGE AC/DC CONVERTER

A. CONFIGURATION OF THE PROPOSED AC-DC CONVERTER

The topology of the programmable AC power supply is shown in Fig.1. It consists of two part: AC-DC rectifier and DC-AC inverter. The proposed single-phase single-stage isolated bridgeless AC-DC PFC converter is applied to AC-DC rectifier part. For inverter part, two single-phase full-bridge inverters would be connected in series or parallel for high or low output voltage applications because of the wide range AC output voltage. Therefore, the secondary side of the isolated AC-DC converter's transformer has two windings for two independent output voltages. Since the two windings are identical, just only one winding is taken into consideration to simplify the analysis. The simplified circuit of the proposed single-phase single-stage isolated PFC converter is shown in Fig.2.

The proposed AC-DC topology is comprised of bridgeless rectifier diodes, series resonance circuit, active-clamped circuit, HF transformer and output rectifier diodes circuit. The bridgeless rectifier topology consists of two main power switches S_1, S_2 and two diodes D_1, D_2, and the two power

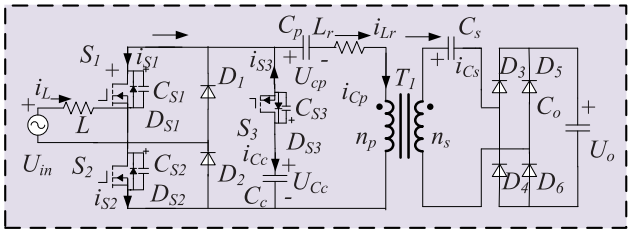

FIGURE 2. Simplified circuit of the proposed single-phase single-stage isolated PFC converter topology.

switches are driven by the same logical pulse width modulation(PWM) signal. The auxiliary power switch S_3 and clamp capacitor C_c is composed of active-clamped circuit, and it could limit the voltage stress of main power switches. The inductor L_r, capacitor C_p on the primary side and capacitor C_s on the secondary side of HP transformer T_1 constitute the series resonant circuit. By designing the parameters of resonant circuit reasonably, ZVS turn-on of the main switches S_1, S_2 and auxiliary switch S_3 and ZCS turn-off of output rectifier diodes could be realized. In order to improve power density and conversion efficiency, SiC MOSFETs are used for power switches. D_{Sx} and C_{sx} represent the anti-parallel diode and parasitic capacitor of the power switch S_x respectively, where $x = 1, 2$ and 3.

B. OPERATION PRINCIPLE

In order to simplify the theoretical analysis, the following assumptions are made:

(i) As the switching frequency f_s is much higher than the AC input voltage frequency f_g, it is assumed that the AC input voltage is constant within each switching frequency.

(ii) Input inductor L, resonant capacitors C_p and C_s, resonant inductor L_r, clamping capacitor C_c and output capacitor C_o are ideal components, and C_p,$C_s \ll C_c$, $L_r \ll L$.

(iii) The HF transformer is also an ideal electrical component, and the turns ratio of primary and secondary side satisfies n_p:n_s= n:1.

(iv) Output filter capacitor C_o and clamping capacitor C_c are large enough, and the values of output voltage U_o and clamped capacitor voltage U_{Cc} almost remain unchanged within each switching period.

(v) The resonant inductor L_r and equivalent capacitor C_r constitute the series resonant circuit, where capacitor C_p and C_s consists of resonant capacitor C_r, and $f_r = 1/(2\pi\sqrt{L_r C_r})$. Resonant frequency f_r is higher than the switching frequency f_s. In order to facilitate designation of the controller and realize the soft-switching operation of the power devices, the conduction time of the main power switches S_1 and S_2 must satisfied $T_{on} \geq 0.5T_r$, where $T_r = 1/f_r$.

In order to describe the soft-switching process for the power devices, the operation principle will be analyzed in details when the AC input voltage is in the positive half of voltage period, which is shown in Fig.3. When the AC input voltage is in the negative half of voltage period, the situation

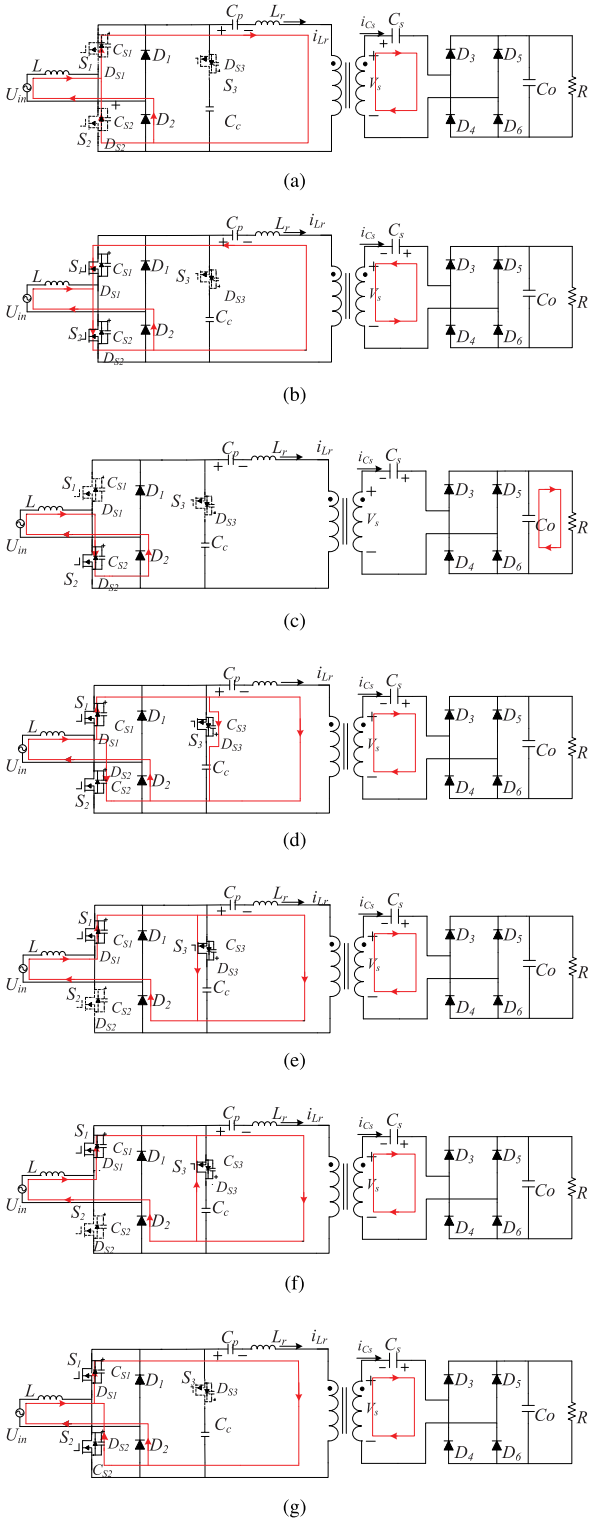

FIGURE 3. Typical operating mode of the proposed single-stage isolated bridgeless converter. (a) Mode 1. (b) Mode 2. (c) Mode 3. (d) Mode 4. (e) Mode 5. (f) Mode 6. (g) Mode 7.

is similar. Assuming that the converter operates in continuous conduction mode(CCM), and there are seven different operating modes. The voltage and current of operation waveforms

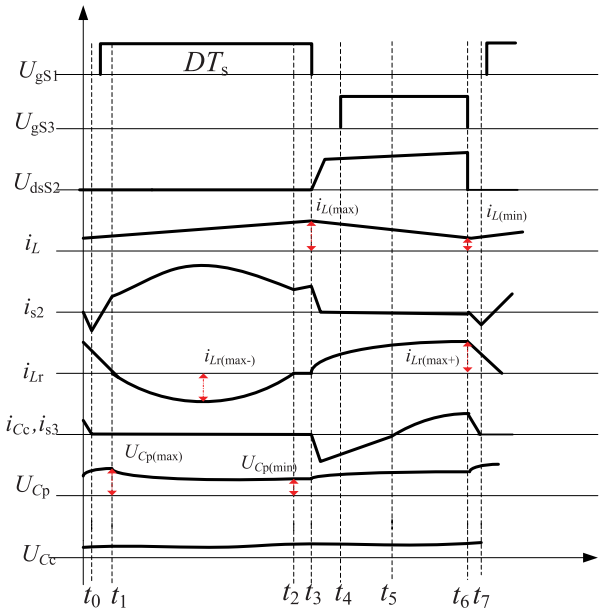

FIGURE 4. Operating waveform of the single-stage bridgeless PFC converter.

are also shown in Fig.4. A detailed description of each operation mode will be given below.

1) MODE 1 (t_0-t_1)

This stage begins when the energy stored by the parasitic capacitor C_{S2} of the main switch S_2 is released. At time t_0, the anti-parallel diode D_{S2} of the main switch S_2 starts to conduct, and the bulk diode D_{S1} of the main switch S_1 has also conducted, ZVS turn-on for both main switches S_1 and S_2 is realized. During this process, auxiliary switch S_3 is turned off, and the output rectifier diodes D_3 and D_6 conducts. At time t_1, the resonant inductor current i_{Lr} becomes zero, the resonant capacitor voltage U_{Cp} reaches the maximum voltage $U_{Cp(max)}$ and ZCS turn-off for the output rectifier diodes D_3 and D_6 also could be realized.

There are two circuit loops on the primary side of the transformer. The first circuit loop consists of AC voltage U_{in}, inductor L, main switch S_1, resonant capacitor C_p, resonant inductor L_r and diode D_2. The other circuit loop consists of main switch S_1, resonant capacitor C_p, resonant inductor L_r and the main switch S_2.

2) MODE 2 (t_1-t_2)

At this stage, main switches S_1 and S_2 remain conduction, auxiliary switch S_3 is still turned-off, and the input inductor L is linearly charged by the AC input voltage U_{in}. As the direction of resonant inductor current i_{Lr} changes, the output rectifier diodes D_4 and D_5 begin to conduct. The current flowing through the main switch S_2 equals to the sum of input inductor current i_L and the resonant inductor current i_{Lr}. The series resonant circuit resonates until the resonant inductor current i_{Lr} becomes zero at time t_2. The input inductor i_L, resonant inductor current i_{Lr} and resonant capacitor voltage U_{Cp} can be expressed as

$$i_L(t) = \frac{U_{in}}{L}(t - t_1) + i_L(t_1) \tag{1}$$

$$i_{Lr}(t) = i_{Lr(max-)}sin(\omega_r(t - t_1)) \tag{2}$$

$$U_{Cp}(t) = i_{Lr(max-)}Z_r cos(\omega_r(t - t_1) - 1) + U_{Cp}(t_1) \tag{3}$$

$$i_{S2}(t) = i_L(t) - i_{Lr}(t) \tag{4}$$

where, $i_{Lr(max-)}$ represents the negative peak value of resonant inductor i_{Lr}, $Z_r = \sqrt{(L_r/C_r)}$, $\omega_r = \sqrt{(L_r C_r)}$, $C_r = C_p C_s/(n^2 C_p + C_s)$.

In this process, resonant capacitor C_p on the primary side of the transformer begins to discharge. As the conduction time of main switch S_2 is greater than or equal to half of the resonant period($T_{on} \geq 0.5T_r$), resonant inductor i_{Lr} becomes zero at time t_2, the resonant capacitor voltage U_{Cp} drops to the minimum value of $U_{Cp(min)}$. The operation principle of the resonant capacitor C_s on the secondary side of transformer is similar to capacitor C_p. The duration of this mode is exactly equal to half of the resonance period($0.5T_r$). The ZCS turn-off for the output rectifier diodes D_4 and D_5 also could be realized.

There are also two circuit loops on the primary side of the transformer. The first circuit loop consists of AC input voltage U_{in}, inductor L, main switch S_2 and diode D_2. The other circuit loop consists of main switch S_1, resonant capacitor C_p,resonant inductor current i_{Lr} and the main switch S_2.

3) MODE 3 (t_2-t_3)

As shown in Fig.3(c), main switch S_2 remains conduction and the inductor L is still charged by the AC input voltage, inductor current i_L continues to increase. As the resonant inductor current i_{Lr} becomes zero, the current flowing through the main switch S_2 is equal to the inductor current i_L. The output filter capacitor C_o on the secondary side of the transformer provides energy for the load. This stage ends at the time t_3, when the main switch S_2 is turned off. The current flowing through the main switch S_2 and the capacitor U_{Cp} can be expressed as

$$i_{S2}(t) = i_L(t) = \frac{U_{in}}{L}(t - t_2) + i_L(t_2) \tag{5}$$

$$U_{Cp}(t) = U_{Cp(t_2)} = U_{Cp(min)} \tag{6}$$

There are only one circuit loop on the primary side of the transformer, and it consists of AC voltage U_{in}, inductor L, main switch S_2 and diode D_2. All the diodes of the rectifier bridge on the secondary side of the transformer are in the off-state.

4) MODE 4 (t_3-t_4)

As shown in Fig.3(d), main switch S_2 is turned off at time t_3, and the auxiliary switch S_3 does not turn on. The inductor current i_L charges the parasitic capacitor C_{S2} of the main switch S_2, and discharges the parasitic capacitor C_{S3} of the auxiliary switch S_3. As the value of parasitic capacitor C_{S3}

is small, the anti-parallel diode D_{S3} will conduct quickly, and the input inductor current i_L also charges the clamping capacitor C_c. The series resonant circuit composed of resonant inductor i_L and equivalent capacitor C_r starts to resonate, the resonant inductor current i_L increases from zero, and the output rectifier diodes D_3 and D_6 start to conduct. The parasitic capacitor voltage U_{Cs2} of the main switch S_2 rises from zero until it reaches the clamping capacitor voltage U_{Cc}. The input inductor current i_L, the drain-source voltage U_{Cs2} of the main switch S_2 and the resonant inductor i_{Lr} are obtained from equations (7),(8) and (9) respectively

$$i_L(t) = \frac{U_{in} - U_{Cc}(t_3)}{L}(t - t_3) + i_L(t_3) \tag{7}$$

$$U_{Cs2}(t) = \frac{i_{S2}}{C_{S2}}(t - t_3) \tag{8}$$

$$i_{Lr}(t) = i_{Lr(max+)}sin(\omega_r(t - t_3)) = i_L(t) - i_{Cc}(t) \tag{9}$$

During this interval, the charging time of parasitic capacitor C_{S2} and discharging time of parasitic capacitor C_{S3} are very short, and the anti-parallel diode D_{S3} of auxiliary switching S_3 starts conduction. As the value of clamping capacitor C_c is much higher than parasitic capacitor C_{S2} and C_{S3}, the capacitor voltage U_{Cc} almost remains constant. The time interval of this stage can be obtained as

$$\Delta t_{34} = t_4 - t_3 = \frac{U_{Cc}C_{S2}}{i_{S2(t_3)}} \tag{10}$$

In order to realize the ZVS turn-on condition for auxiliary switch S_3, the energy stored in inductor L must be greater than that stored in parasitic capacitors C_{S2} and C_{S3}, that is, it must be satisfied

$$L > \frac{(C_{S2} + C_{S3})(U_{Cc}(t_3))^2}{i_L^2(t_3)} \tag{11}$$

There are three circuit loops on the primary side of the transformer. The first circuit loop consists of AC voltage U_{in}, inductor L, main switch S_2 and diode D_2. The secondary circuit loop consists of AC voltage U_{in}, inductor L, main switch S_1, auxiliary switch S_3, clamping capacitor C_c and diode D_2. The third circuit loop consists of AC voltage U_{in}, inductor L, main switch S_1, resonant capacitor C_p, resonant inductor current i_{Lr} and diode D_2.

5) MODE 5 (t_4-t_5)

As shown in Fig.3(e), the driver signal becomes high for auxiliary switch S_3 at time t_4, the ZVS turn-on for auxiliary switch S_3 could be realized because of the conduction of anti-parallel diode D_{S3}. The input inductor current i_L decreases with the slope of $(U_{in} - U_{Cc})/L$, and the clamping capacitor current i_{Cc} becomes zero at time t_5. Since the resonant inductor current i_{Lr} keeps charging the resonant capacitor C_p, the resonant capacitor voltage U_{Cp} increases. The input inductor current i_L can be expressed as

$$i_L(t) = \frac{U_{in} - U_{Cc}(t_4)}{L}(t - t_4) + i_L(t_4) \tag{12}$$

There are also two circuit loops on the primary side of the transformer. The first circuit loop consists of AC voltage U_{in}, inductor L, main switch S_1, auxiliary switch S_3, clamping capacitor C_c and diode D_2. The other circuit loop consists of AC voltage U_{in}, inductor L, main switch S_1, resonant capacitor C_p, resonant inductor i_{Lr} and diode D_2.

6) MODE 6 (t_5-t_6)

As shown in Fig.3(f), when the resonant inductor current i_{Lr} is equal to input inductor current i_L. The current i_{S3} becomes zero and starts to flow from the drain to the source. At time t_6, the auxiliary switch S_3 is turned off, and this stage ends. During the interval, the direction of resonant inductor i_{Lr} is always positive, and the resonant capacitor C_p is always charged. The resonant capacitor voltage U_{Cp} increases, and the diodes of D_3 and D_6 on the secondary side of the transformer conducts.

There are also two circuit loops on the primary side of the transformer. The first circuit loop consists of AC voltage U_{in}, inductor L, main switch S_1, resonant capacitor C_p, resonant inductor i_{Lr} and diode D_2. The other circuit loop consists of auxiliary switch S_3, clamping capacitor C_c, resonant capacitor C_p and resonant inductor i_{Lr}.

7) MODE 7 (t_6-t_7)

As shown in Fig.3(g), at time t_6, auxiliary switch S_3 is turned off, and the resonant inductor current i_{Lr} discharges the parasitic capacitor C_{S2} of main switch S_2 and charges the parasitic capacitor C_{S3} of the auxiliary switch S_3. Resonant inductor current i_{Lr} begins to decrease, but the direction remains positive. In order to ensure the ZVS turn-on for the main switch S_2, the parasitic capacitor voltage U_{Cs2} needs to be zero before the end of this stage to enable the conductions of the anti-parallel diode D_{S2}. Therefore, the electric energy stored in the resonant inductor i_{Lr} must be larger than that stored in the parasitic capacitor C_{S2}, so that the energy stored in the parasitic capacitor C_{S2} is completely released. The resonant inductor L_r must meet the following requirements

$$L_r > \frac{(C_{S2} + C_{S3})(U_{Cc}(t_6))^2}{i_{Lr}^2(t_6)} \tag{13}$$

At time t_7, as the conduction of anti-parallel diode D_{S2}, ZVS turn-on condition can be achieved for main switch S_2 if the driver signal becomes high level, and the next switch period begins.

There are also two circuit loops on the primary side of the transformer. The first circuit loop consists of AC voltage U_{in}, inductor L, main switch S_1, resonant capacitor C_p, resonant inductor i_{Lr} and diode D_2. The other circuit loop consists of auxiliary switch S_1, resonant capacitor C_p, resonant inductor i_{Lr} and main switch S_2.

It should be noted that when the input grid voltage or load changes, some of the power devices may not work in the soft-switching condition, and the corresponding working mode would be slightly different, but overall the operation process is similar. In order to avoid repetition, it will not be described

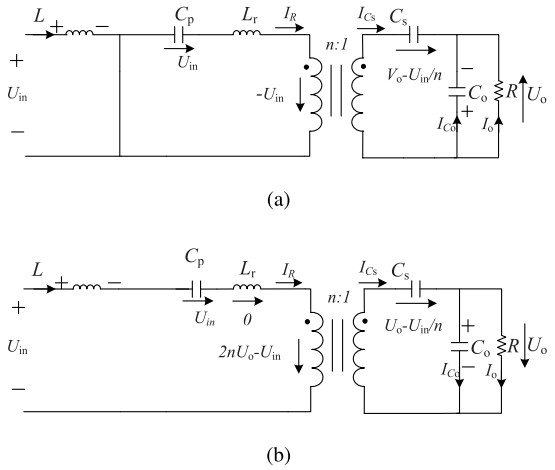

FIGURE 5. Equivalent circuit of the proposed single-stage isolated converter. (a) When main switch S_2 is turned on. (b) When main switch S_2 is turned off.

in details here. The soft-switching operation condition for the power switches will be introduced in the following section.

III. STEADY-STATE ANALYSIS

A. VOLTAGE GAIN

In this section, the voltage gain of the proposed topology will be discussed for details. When the AC voltage U_{in} is positive, the equivalent circuit of the proposed topology could be simplified as shown in Fig.5. Fig.5(a) and (b) present the the equivalent circuit of the main switch S_2 in on-state or off-state respectively. When the main switch S_2 is turned off, as the clamping capacitor C_c is relatively large, the clamped capacitor voltage U_{Cc} is almost constant during this interval, and the current i_{Cc} is close to zero, so the clamped circuit can be ignored for simplicity. When the main switch S_2 is in the conduction state as shown in Fig.5(a), the voltage at both ends of the inductor L is U_{in}, and the products of volt-seconds is $U_{in}DT_s$. Where, D and T_s represent the duty ratio of the main switch S_2 and switch period respectively. When the main S_2 is in the off state as shown in Fig.5(b), the resonant inductor L_r is in series with C_r, and the average voltage at both end of the resonant inductor i_{Lr} is zero. Similarly, the product of the volt-seconds at both ends of the inductor L can be expressed as $(2nU_0 - U_{in})(1 - D)T_s$. Based on the principle of volt-seconds balance of the input inductor L, equation (14) can be obtained as

$$U_{in}DT_s = (2nU_0 - U_{in})(1 - D)T_s \tag{14}$$

and the ratio of output voltage U_o to input voltage U_{in} can be obtained as

$$\frac{U_o}{U_{in}} = \frac{1}{2n(1 - D)} \tag{15}$$

When the AC voltage U_{in} is negative, the same expression of voltage gain can be obtained based on the similar analytical method, and the voltage gain M of the proposed topology is expressed as

$$M = \frac{U_o}{|U_{in}|} = \frac{1}{2n(1 - D)} \tag{16}$$

B. ZVS AND ZCS CONDITION

Based on the analysis of the aforementioned section II, in order to realize the ZVS turn-on of the main switch S_2, the energy stored in resonant L_r should fully charge the parasitic capacitor C_{S2} of the main switch S_2 and discharge the parasitic capacitor C_{S3} of switch S_3, and enable the anti-parallel diode D_{S2} of the main switch S_2 to conduct. In this case, the current flowing through the main switch S_2 should meet the requirement of $i_{S2}(t_0) = i_L(t_0) - i_{Lr}(t_0) < 0$, which satisfies equation (17) and (18).

$$\begin{aligned} i_{S2}(t_0) &= i_{L(min)} - i_{Lr}(t_0) \\ &= \frac{P_o}{U_{in}} - \frac{DT_sU_{in}}{2L} - i_{Lr(max+)} \\ &= \frac{P_o}{U_{in}} - \frac{DT_sU_{in}}{2L} - \frac{I_o}{4nC_rf_sZ_r} \\ &\quad \times sin(\omega_r(1 - D)T_s) \end{aligned} \tag{17}$$

$$\begin{aligned} &\frac{1}{2}(L_ri^2_{Lr(max+)} - Li^2_{L(min)}) \\ &\quad \geq \frac{1}{2}(C_{S2} + C_{S3})U^2_{Cc} \end{aligned} \tag{18}$$

The situation for switch S_1 is similar when input AC voltage U_{in} is negative. In order to realize the ZVS turn-on condition for auxiliary switch S_3, the current i_L stored in the inductor L discharges the parasitic capacitor C_{S3} of the auxiliary switch S_3 and charges the parasitic capacitor C_{S2} of the main switch S_2, and enables the anti-parallel diode D_{S3} of the auxiliary switch S_3 to conduct, which satisfies equation(19) and (20).

$$\begin{aligned} i_{S3}(t_3) &= i_L(t_3) - i_{Lr}(t_3) \\ &= i_{L(max)} \\ &= \frac{P_o}{U_{in}} + \frac{DT_sU_{in}}{2L} \end{aligned} \tag{19}$$

$$\frac{1}{2}Li^2_{L(max+)} \geq \frac{1}{2}(C_{S2} + C_{S3})U^2_{Cc} \tag{20}$$

In fact, at time t_3, resonant inductor current i_{Lr} is zero, and equation(20) can be easily satisfied with large input inductor L and small parasitic capacitor C_{S2},C_{S3}. The ZVS condition for auxiliary S_3 can be realized nearly in overall load range. equation(18) may not be satisfied with a small resonant inductor L_r or light load. With large resonant inductor L_r and small input inductor L may extend the ZVS range, but it would lead to large ripple current of i_L, and it should be chosen based on the tradeoff between power losses and current ripple of the whole system.

The ZCS condition for output rectifier diodes can be easily deduced according to mode 1 and 2 in section II. When the nonconduction time of the switch S_1 or S_2 is greater than half of the resonance period, D_3 and D_6 can work in ZCS

condition, which satisfies

$$T_{off\_min} = (1 - D_{max})T_s = (\frac{|U_{in}|}{nU_o})T_s \geq \frac{1}{2}T_r \quad (21)$$

Similarly, the ZCS operation condition of diodes D_4 and D_5 can be obtained based on equation (22)

$$T_{on\_min} = D_{min}T_s = (1 - \frac{|U_{in}|}{nU_o})T_s \geq \frac{1}{2}T_r \quad (22)$$

where, D, T_s and T_r represent the duty ratio of switch S_1 or S_2, switching period and resonant period respectively.

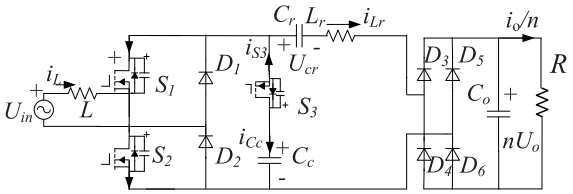

FIGURE 6. Equivalent circuit with the secondary quantities are referred to the primary.

C. VOLTAGE STRESS ANALYSIS

In order to simplify the analysis, the winding on the secondary side of the HF frequency is referred to the primary side, and the equivalent circuit is obtained as shown in Fig.6. The maximum voltage stress of the main switch can be expressed as

$$U_{S1(max)} = U_{S2(max)} = 2nU_o + U_{Cr(max)} \quad (23)$$

When the system works stably, the current flowing through the diodes of $I_{D4(avg)}$ and $I_{D5(avg)}$ satisfies that

$$\begin{aligned} I_{D4(avg)} &= I_{D5(avg)} = \frac{I_o}{2n} \\ &= \frac{1}{T_s}\int_{t_1}^{t_2}\frac{1}{Z_r}U_{Cr(max)}sin(\omega_r t)dt \\ &= \frac{1}{T_s}\int_{0}^{\frac{1}{2}T_r}\sqrt{\frac{C_r}{L_r}}U_{Cr(max)}sin(\omega_r t)dt \end{aligned} \quad (24)$$

And $U_{Cr(max)}$ also can be deduced from equation (24)

$$U_{Cr(max)} = \frac{I_o}{4nC_r f_s} \quad (25)$$

It can be easily analyzed that the maximum voltage stress of auxiliary switch S_3 satisfies

$$U_{S3(max)} = U_{Cc(max)} = \frac{|U_{in(max)}|}{1 - D} \quad (26)$$

The maximum voltage stress of diode D_1 and D_2 also can be derived as the equation (26).It is also easy to conclude that the voltage stress of rectifier diodes $D_3 \sim D_6$ on the secondary side of the transformer are always equal the output voltage U_o regardless of the duty ratio D.

$$U_{D1(max)} = U_{D2(max)} = U_{Cc(max)} \quad (27)$$

$$U_{D3(max)} = U_{D5(max)} = U_o \quad (28)$$

TABLE 1. Design specifications.

Parameter	Value
AC input voltage range,U_{in}	175∼265V
AC input frequency range,f_g	47∼53Hz
Input current ripple,$I\%$	20%
Ouput voltage ripple,$\delta\%$	5%
Turns ratio of the transformer ,n	6:7
DC ouput voltage ,U_o	300 V
Rated power,P_o	3000W

IV. DESIGN CONSIDERATION

In this section, the design consideration of the proposed single-stage PFC converter is presented, and the detailed specifications of the bridgeless AC-DC PFC converter is shown in Table 1.

A. CHOSEN OF KEY COMPONENT

1) INPUT INDUCTOR L AND OUTPUT CAPACITOR C_o

Assuming that the current ripple $I\%$ of the inductor is 20% and the converter operates in CCM mode. Ignoring the power losses and based on the equality of AC input power and DC output power, it is easy to calculate the inductance value as follows:

$$L = \frac{U_{in\_min(peak)}D_{min}}{f_s I_{Lmax(peak)}I\%} = 441uH \quad (29)$$

If the output voltage ripple is $\delta\% = 5\%$, the capacitance value of the output filter capacitor C_o can be easily calculated according the equation(30)

$$C_o = \frac{P_o}{4f_g U_o^2 \delta\%} = 3333uF \quad (30)$$

Finally, standard values of the inductor $L = 450uH$ and capacitor $C_o = 3300uF$ are chosen for the experimental prototype.

2) RESONANT INDUCTOR i_{Lr}, RESONANT CAPACITOR C_r AND CLAMPING CAPACITOR C_c

The resonant circuit is the core of the whole converter, which is composed of resonant inductor i_{Lr}, resonant capacitor C_p and C_s. Reasonable desiganization of resonant parameters can not only ensure the normal operation of the main circuit, but also enable the power devices of the converter to work in soft switching condition.

The selection of resonant inductor L_r should ensure that the main switch S_1 and S_2 can realize ZVS turn-on operation, which satisfies equation (18) and (20). Finally, $L_r = 5uH$ and $C_r = 0.52uF$ are chosen for the resonant circuit, where $C_r = \frac{C_p C_s}{n^2 C_p + Cs}$, $C_p = 2.2uF$, $C_s = 0.5uF$ and $n = 6/7$. The resonant frequency can be calculated as $f_r = \frac{1}{2\pi\sqrt{L_r C_r}} =$ 98.7kHz. Meanwhile, as the conduction time of the main switch S_2 or S_1 satisfies $T_{on} \geq 0.5T_r$, and the soft switching condition for the power components could be realized.

About the selection of clamping capacitor C_c, it is expected that the value of the clamping capacitor would be as large as possible, so that the voltage U_{Cc} of clamping capacitor will remain basically unchanged during the switch period T_s.

However, the clamping capacitor with an excessive capacity will make the volume of the converter too large. In addition, based on the operation mode 6 mentioned in section II, resonant inductor L_r, resonant capacitor C_r and clamping capacitor C_c will actually resonants when the auxiliary switch S_3 turns off. Without considering the effect of clamping capacitor C_c for the main circuit, the value of the clamping capacitor C_c must be much greater than that of resonant capacitor C_r, so $C_c = 50uF$ is chosen for the clamping circuit. As a result of $C_c \gg C_r$, the voltage U_{Cc} of clamping capacitor C_c keeps almost constant during the switch period.

3) HF TRANSFORMER

The transformer must be designed to transfer the instantaneous input power of 3kW at the conditions of 85kHz switching frequency and 300V output voltage. Based on the analysis mentioned in section II, as the existence of capacitors C_p and C_s in the primary and secondary side of the transformer, there is no DC voltage component, it would greatly reduce the volume of the transformer. The transformer is composed of EE55 magnetic core, and two magnetic core are stacked to increase the core area as shown in Fig.7. The copper foil is used for the primary and secondary-side windings, and the size is $0.1mm$ (thickness)*$27mm$ (width). The secondary side of the transformer has two windings, and they are connected in series when the output AC voltage of the corresponding inverter is between 150V and 300V, when output voltage of AC source is lower than 150V, these two wings are connected in parallel. The turns of primary and secondary-side are 6 and 7 respectively. Some key components for the PFC converter are shown in Table.2.

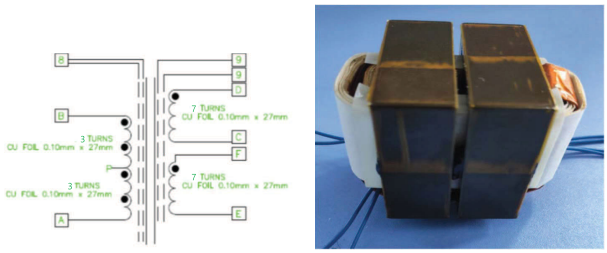

(a) (b)

FIGURE 7. HF tranformer. (a) Winding diagram. (b) Physical model.

TABLE 2. Key components for the PFC converter.

Parameter	Value
Input inductor,L	450uH
Resonant inductor,L_r	5uH
Primary resonant capacitor,C_p	2.2uF
Secondary resonant capacitor,C_s	0.5uF
Output filter capacitor ,C_o	2200uF
Sic Power MOSFETs ,$S_1 \sim S_3$	C3M006509J
Diodes,$D_1 \sim D_2$	C4D30120D
Diodes,$D_3 \sim D_6$	RHRP1560

B. CONTROL STRATEGY

The control block diagram of the proposed bridgeless isolated PFC rectifier is shown in Fig.8, and the three electrical

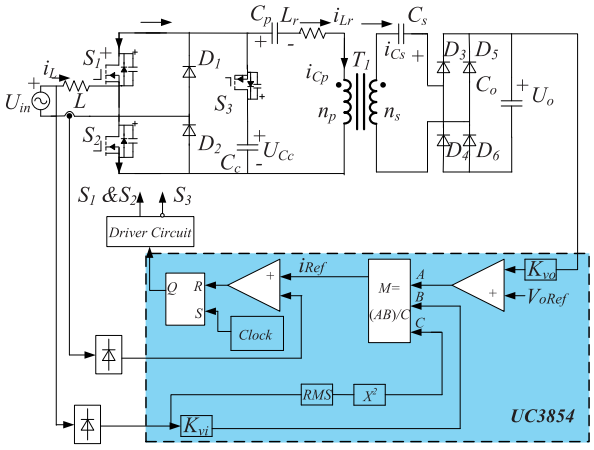

FIGURE 8. Control block diagram of the single-stage PFC converter.

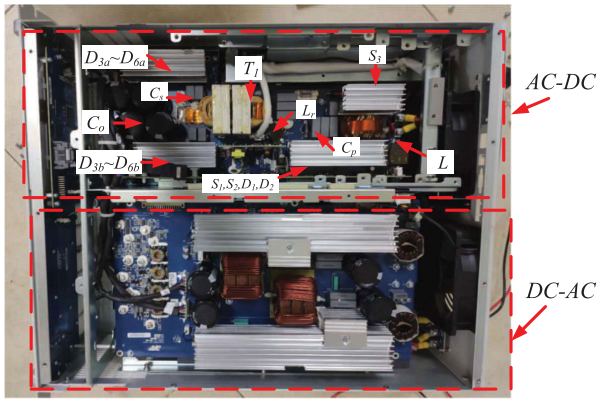

FIGURE 9. Experimental prototype of the single-stage PFC converter.

parameters of input AC voltage U_{in}, inductor current i_L and output voltage U_o are measured respectively, it is not necessary to sense the positive or negative AC voltage cycle. The driver logic signals for main switches of S_1 and S_2 are same, and the driver signal of auxiliary switch S_3 is complementary to them. A standard PFC IC UC3854 could be chosen for the controller, which uses average current-mode control to accomplish fixed-frequency current control with stability and low distortion of grid current.

V. EXPERIMENTAL RESULTS

In order to verify the correctness and feasibility of the proposed sing-stage isolated bridgeless PFC converter topology and its operation principle, a 3kW experimental prototype based on SiC power device is built as shown in Fig.9. The HF transformer has two wings with rectifier diodes on the secondary side and they are connected in parallel. Due to the high switch frequency of the SiC power devices, the standard low-cost IC of UC3854 is chosen as the controller.

Experimental waveforms are measured at rated input AC voltage of 220V and output power of 3kW resistance load. Fig.10 shows the measured experimental waveform of input

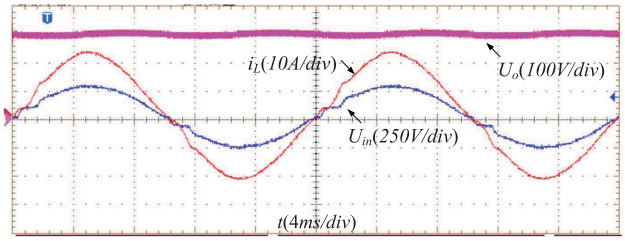

FIGURE 10. Experimental waveforms of input AC voltage U_{in}, input inductor current i_L and output capacitor voltage U_o.

AC voltage U_{in}, input inductor current i_L and output capacitor voltage U_o, it can be observed that the input inductor current is sinusoid and in phase with the input voltage, and the output capacitor voltage is stable at 300V. The input power factor and the THD value of grid current are measured by analyzer Tek PA3000, the PF value is as high as 0.995, and the THD value is 3.9 %, it also can meet IEC 61000-3-2 standard.

The voltage of resonant capacitor C_p in the primary side and the capacitor C_s in the secondary side of HF transformer is measured as shown in Fig.11. Capacitor voltage U_{Cp} and U_{Cs} have the same phase angles, and the phase and amplitude of the capacitor voltage U_{Cp} is almost same with the rectifier AC input voltage $|U_{in}|$, which is consistent with the analysis of equivalent circuit in steady-state operation as shown in Fig.5.

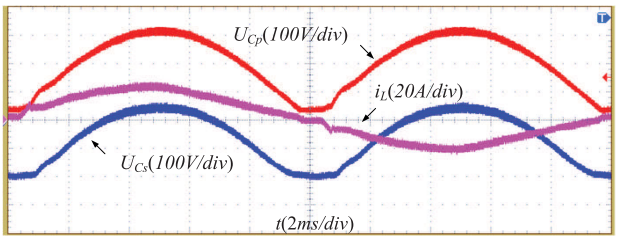

FIGURE 11. Experimental waveforms of resonant capacitor voltage U_{Cp} in primary side, input inductor current i_L and resonant capacitor voltage U_{Cs} in secondary side.

The experimental waveforms of ZVS turn-on operation for main switches S_1, S_2 are shown in Fig.12. When the driver signal of the main switches become high, the voltage between the drains and sources have been reduced to zero due to the conduction of anti-parallel diodes, thus the ZVS turn-on operation of the main switches can be realized. The soft-switch operation principle of the auxiliary S_3 is similar, and the ZVS turn-on waveform is shown in Fig.13.

The soft switching waveform of output rectifier diodes D_3 and D_5 in the secondary side of HF transformer is shown in Fig.14. The voltage waveforms of anode and cathode and the conduction current waveform for the rectifier diodes D_3 and D_5 are shown in Fig.14(a) and Fig.14(b) respectively. Due to the change of direction of resonant inductor i_{Lr} within a switching cycle, the ZCS turn-off operation of the output rectifier diodes $D_3 \sim D_6$ can be achieved.

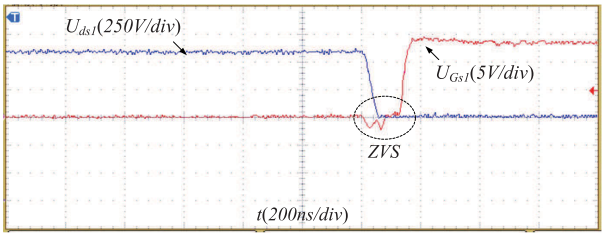

(a)

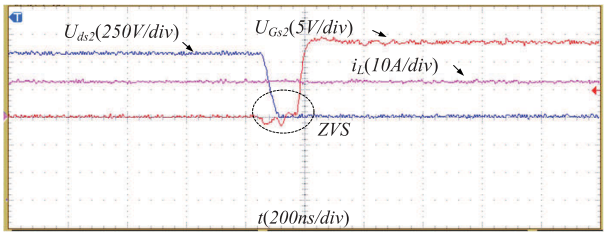

(b)

FIGURE 12. Experimental waveform of soft switching operation for power switches S_1 and S_2. (a) ZVS turn-on for main switch S_1. (b) ZVS turn-on for main switch S_2.

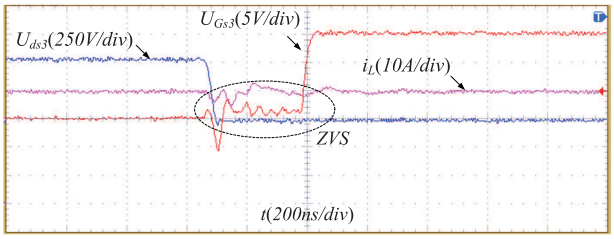

FIGURE 13. Experimental waveform of ZVS turn-on for auxiliary switch S_3.

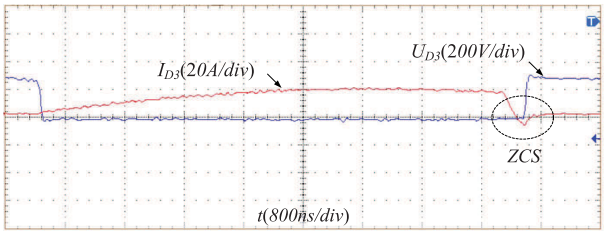

(a)

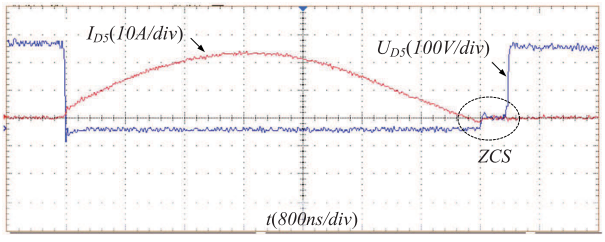

(b)

FIGURE 14. Experimental waveform of ZCS operation for output rectifier diodes D_3 and D_5. (a) ZCS turn-off for diode D_3. (b) ZCS turn-off for diode D_5.

The conversion efficiency of the proposed single-stage isolated converter is measured by Tektronix PA3000. As the two-stage PFC topology proposed in [5] is widely

TABLE 3. Performance comparison.

Reference	Input voltage range	Output voltage range	Output Power	Switch frequency	Number of switches	Number of magnetic components	Peak efficiency	Control complexity	Cost
Ref.[5]	85∼265V	200∼450V	3.3kW	200kHz	6 MOSFETs, 11 diodes	4	93.6%	Complexity	High
Ref.[21]	220V	240V	1.6kW	25kHz	1 MOSFETs, 5 diodes	3	91%	Simple	Low
Ref.[22]	120V	220∼336V	1.5kVA	100kHz	8 MOSFETs	4	96.5%	Simple	Medium
Ref.[23]	208V	400V	3kW	10kHz	5 MOSFETs, 13 diodes	2	94%	Simple	High
Ref.[24]	207∼253V	280∼420V	3.3kW	20∼ 120kHz	8 MOSFETs	3	95%	Complexity	Medium
Ref.[25]	220V	60V	1.4kW	50kHz	8 MOSFETs, 4 diodes	3	96%	Simple	Medium
Ref.[26]	220V	320∼400V	3.3kW	100kHz	10 MOSFETs	4	96.7%	Complexity	High
Proposed	175∼265V	300V	3kW	85kHz	3 MOSFETs, 4 diodes	3	95.7%	Simple	Low

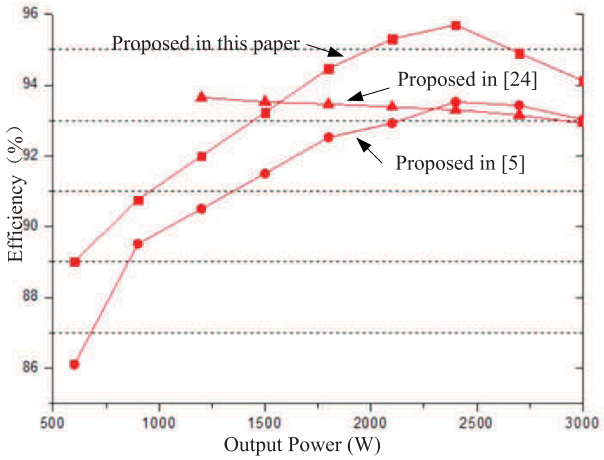

FIGURE 15. Comparison of conversion efficiency with different topologies at rated input voltage.

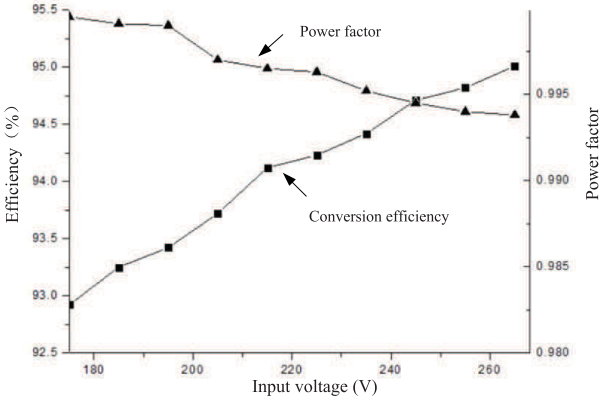

FIGURE 16. Measured efficiency curve and PF with different input voltage at 3 kW load condition.

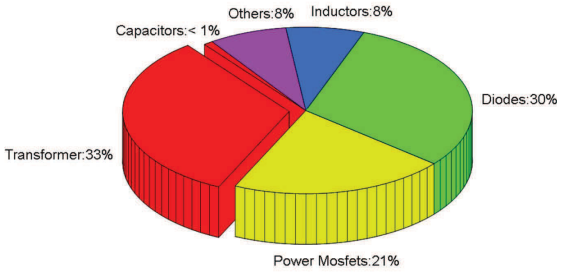

FIGURE 17. Loss analysis of the proposed PFC converter at rated power.

implemented in programmable AC source applications at present, and it is compared with the proposed single-stage isolated converter. Meanwhile, the 3kW single-stage isolated ZCS current-fed full-bridge converter recently proposed in [23] is also chosen for comparison as shown in Fig.15. The conversion efficiency of the proposed single-stage topology is significantly higher than the other two topologies, and a peak efficiency of 95.7 % could be achieved.

The measured efficiency curve and PF value with different input voltage at 3kW load condition are provided in Fig.16. Nearly unity PF can be achieved and a high performance of conversion efficiency is obtained over the entire range of input voltage.

Fig.17 shows the power loss analysis of the components at rated power when input voltage is 220V, and the loss calculation method for each component is routine [23], [24], [27], [28]. All the results are at 85kHz switching frequency, and the power losses will be lower with higher switching frequency. As the ZVS turning-on condition for power MOSFETs, the switching losses can be minimized, and with the ZCS turning-off condition for output rectifier diodes, the snubber circuit is small or not necessary, this also improves the conversion efficiency of the converter. The majority of the power losses comes from the transformer, diodes and power switches.

Table 3 shows the comparison between the proposed single-stage birdgeless isolated PFC converter with the presented isolated AC-DC converter in [5], [21], [22], [23], [24], [25] and [26], and the comparison results show that the

topology proposed in this paper demonstrates a good performance for single-phase high-power applications based on the tradeoff of the cost, control complexity and the conversion efficiency.

VI. CONCLUSION

In this paper, a single-stage bridgeless isolated AC-DC converter topology with PFC is proposed for programmable AC power source applications. The ZVS turn-on of main and auxiliary switches and ZCS turn-off of output rectifier diodes can be realized based on LC series-resonant technology and active-clamping method under certain load conditions. Finally, a 3kW experimental prototype based on SiC power devices is built to verify the correctness and feasibility of the topology, 95.7% of peak conversion efficiency and 3.9% of grid THD current can be achieved. Some features of the proposed single-stage isolated converter can be summarized as follows:

1) Low cost and high energy conversion efficiency of the proposed converter can be achieved because of few components needed, elimination of the diode rectifier bridge, ZVS turn-on for power switches and ZCS turn-off for output diode rectifier bridge.

2) There is no need to detect the positive and negative half cycle of AC input voltage as the two main switches are driven by the same logic PWM signals.

3) The control circuit is simple and it could be easily implemented by low cost MCU or available analog IC(UC3854).

The single-stage bridgeless converter topology proposed in this paper can provide constant output voltage, low THD value of grid current and nearly unity PF for programmable AC power source applications with galvanic isolation, and it can also be used in other applications, such as battery charges, uninterruptable power supply, etc.

REFERENCES

[1] B. Singh, B. N. Singh, A. Chandra, K. Al-Haddad, A. Pandey, and D. P. Kothari, "A review of single-phase improved power quality AC-DC converters," *IEEE Trans. Ind. Electron.*, vol. 50, no. 5, pp. 962–981, Oct. 2003.

[2] M. M. Jovanovic and Y. Jang, "State-of-the-art, single-phase, active power-factor-correction techniques for high-power applications—An overview," *IEEE Trans. Ind. Electron.*, vol. 52, no. 3, pp. 701–708, Jun. 2005.

[3] S. Dusmez, X. Li, and B. Akin, "A fully integrated three-level isolated single-stage PFC converter," *IEEE Trans. Power Electron.*, vol. 30, no. 4, pp. 2050–2062, Apr. 2015.

[4] B. Poorali and E. Adib, "Analysis of the integrated SEPIC-flyback converter as a single-stage single-switch power-factor-correction LED driver," *IEEE Trans. Ind. Electron.*, vol. 63, no. 6, pp. 3562–3570, Jun. 2016.

[5] D. S. Gautam, F. Musavi, M. Edington, W. Eberle, and W. G. Dunford, "An automotive onboard 3.3-kW battery charger for PHEV application," *IEEE Trans. Veh. Technol.*, vol. 61, no. 8, pp. 3466–3474, Oct. 2012.

[6] F. Musavi, W. Eberle, and W. G. Dunford, "A high-performance single-phase bridgeless interleaved PFC converter for plug-in hybrid electric vehicle battery chargers," *IEEE Trans. Ind. Appl.*, vol. 47, no. 4, pp. 1833–1843, Jul. 2011.

[7] B. Whitaker, A. Barkley, Z. Cole, B. Passmore, D. Martin, T. R. McNutt, A. B. Lostetter, J. S. Lee, and K. Shiozaki, "A high-density, high-efficiency, isolated on-board vehicle battery charger utilizing silicon carbide power devices," *IEEE Trans. Power Electron.*, vol. 29, no. 5, pp. 2606–2617, May 2014.

[8] H.-S. Kim, M.-H. Ryu, J.-W. Baek, and J.-H. Jung, "High-efficiency isolated bidirectional AC–DC converter for a DC distribution system," *IEEE Trans. Power Electron.*, vol. 28, no. 4, pp. 1642–1654, Apr. 2013.

[9] C. Wei, J. Shao, B. Agrawal, D. Zhu, and H. Xie, "New surface mount SiC MOSFETs enable high efficiency high power density bi-directional on-board charger with flexible DC-link voltage," in *Proc. IEEE Appl. Power Electron. Conf. Expo. (APEC)*, Mar. 2019, pp. 1904–1909.

[10] C. Shi, H. Wang, S. Dusmez, and A. Khaligh, "A SiC-based high-efficiency isolated onboard PEV charger with ultrawide DC-link voltage range," *IEEE Trans. Ind. Appl.*, vol. 53, no. 1, pp. 501–511, Jan. 2017.

[11] L. Huber and M. M. Jovanovic, "Single-stage, single-switch, isolated power supply technique with input-current shaping and fast output-voltage regulation for universal input-voltage-range applications," in *Proc. Appl. Power Electron. Conf. (APEC)*, vol. 1, Feb. 1997, pp. 272–280.

[12] J.-J. Lee, J.-M. Kwon, E.-H. Kim, W.-Y. Choi, and B.-H. Kwon, "Single-stage single-switch PFC flyback converter using a synchronous rectifier," *IEEE Trans. Ind. Electron.*, vol. 55, no. 3, pp. 1352–1365, Mar. 2008.

[13] H. S. Athab and D. D.-C. Lu, "A high-efficiency AC/DC converter with quasi-active power factor correction," *IEEE Trans. Power Electron.*, vol. 25, no. 5, pp. 1103–1109, May 2010.

[14] Q. Luo, J. Huang, Q. He, and K. Ma, "Analysis and design of a single-stage isolated AC-DC LED driver with a voltage doubler rectifier," *IEEE Trans. Ind. Electron.*, vol. 64, no. 7, pp. 5817–5907, Jul. 2017.

[15] H. Khalilian, H. Farzanehfard, E. Adib, and M. Esteki, "Analysis of a new single-stage soft-switching power-factor-correction LED driver with low DC-bus voltage," *IEEE Trans. Ind. Electron.*, vol. 65, no. 5, pp. 3858–3865, May 2018.

[16] G. Zhang, J. Zeng, S. S. Yu, W. Xiao, B. Zhang, S.-Z. Chen, and Y. Zhang, "Control design and performance analysis of a double-switched LLC resonant rectifier for unity power factor and soft-switching," *IEEE Access*, vol. 8, pp. 44511–44521, 2020.

[17] S.-W. Lee and H.-L. Do, "Single-stage bridgeless AC–DC PFC converter using a lossless passive snubber and valley switching," *IEEE Trans. Ind. Electron.*, vol. 63, no. 10, pp. 6055–6063, Oct. 2016.

[18] W. Y. Choi and J. S. Yoo, "A bridgeless single-stage half-bridge AC/DC converter," *IEEE Trans. Power Electron.*, vol. 26, no. 12, pp. 3884–3895, Dec. 2011.

[19] N. Golbon and G. Moschopoulos, "A low-power AC–DC single-stage converter with reduced DC bus voltage variation," *IEEE Trans. Power Electron.*, vol. 27, no. 8, pp. 3714–3724, Aug. 2012.

[20] Y. Wei, Q. Luo, J. M. Alonso, and A. Mantooth, "A magnetically controlled single-stage AC–DC converter," *IEEE Trans. Power Electron.*, vol. 35, no. 9, pp. 8872–8877, Sep. 2020.

[21] S. Dian, X. Wen, S. Zhang, and X. Deng, "Digital control of isolated CUK power factor correction converter under wide range of load variation," *IET Power Electron.*, vol. 8, no. 1, pp. 142–150, Jan. 2015.

[22] U. R. Prasanna, A. Kumar Singh, and K. Rajashekara, "Novel bidirectional single-phase single-stage isolated AC–DC converter with PFC for charging of electric vehicles," *IEEE Trans. Transport. Electrific.*, vol. 3, no. 3, pp. 536–544, Sep. 2017.

[23] C. Li, Y. Zhang, Z. Cao, and D. Xu, "Single-phase single-stage isolated ZCS current-fed full-bridge converter for high-power AC/DC applications," *IEEE Trans. Power Electron.*, vol. 32, no. 9, pp. 6800–6812, Sep. 2017.

[24] F. Jauch and J. Biela, "Combined phase-shift and frequency modulation of a dual-active-bridge AC–DC converter with PFC," *IEEE Trans. Power Electron.*, vol. 31, no. 12, pp. 8387–8397, Dec. 2016.

[25] D. Sha and S. Wang, "A single-stage natural power factor corrector based on dual active bridge DC–DC converter without inner current tracking loop," *IEEE Trans. Power Electron.*, vol. 36, no. 1, pp. 342–352, Jan. 2021.

[26] H. Belkamel, H. Kim, and S. Choi, "Interleaved totem-pole ZVS converter operating in CCM for single-stage bidirectional AC–DC conversion with high-frequency isolation," *IEEE Trans. Power Electron.*, vol. 36, no. 3, pp. 3486–3495, Mar. 2021.

[27] C. Li and D. Xu, "Family of enhanced ZCS single-stage single-phase isolated AC–DC converter for high-power high-voltage DC supply," *IEEE Trans. Ind. Electron.*, vol. 64, no. 5, pp. 3629–3639, May 2017.

[28] Z. Liu, J. Liu, and J. Li, "Modeling, analysis, and mitigation of load neutral point voltage for three-phase four-leg inverter," *IEEE Trans. Ind. Electron.*, vol. 60, no. 5, pp. 2010–2021, May 2013.

ZHI ZHANG received the B.S. degree in automation from Xiangtan University, Xiangtan, China, in 2003, the M.S. degree in power electronics and power drives from Guangxi University, Nanning, China, in 2007, and the Ph.D. degree in power electronics and power drives from the South China University of Technology, Guangzhou, China, in 2010.

From 2010 to 2013, he was a Senior Application Engineer with East Group Company Ltd., China. Since May 2013, he has been an Associate Professor with the Department of Electrical Engineering, Dongguan University of Technology, Dongguan, China. From April 2018 to April 2019, he was a Visiting Associate Professor with the Department of Electrical Engineering and Computer Science, Case Western Reserve University, Cleveland, OH, USA. His current research interests include digital control and modulation method of uninterruptable power supplies, photovoltaic inverter systems, grid-connected inverters, dc–dc converters, and soft-switching techniques.

JUNKAI WU received the B.S. degree in electrical engineering from the Guangdong University of Technology, Guangzhou, China, in 2018. He is currently pursuing the master's degree in electrical engineering with the Dongguan University of Technology. His current interests include seamless switching technology of micro-grid and virtual synchronous generator technology.

LIWEI MENG received the B.S. degree in electrical engineering from the Guangdong University of Petrochemical Technology, Maoming, China, in June 2016, and the M.S. degree in electrical engineering from the Guangdong University of Technology, Guangzhou, China, in July 2020. Since June 2020, he has been a Hardware Engineer with Hynn Group Company Ltd., China. His current interests include dc–dc converter, ac-dc-ac converter, and soft-switching techniques.

ZHAOYUN ZHANG (Senior Member, IEEE) was born in Yichang, Hubei, China, in 1977. He received the B.S., M.S., and Ph.D. degrees in electrical engineering from the Huazhong University of Science and Technology, China.

XIAO TANG received the B.S. degree in automation from Central South University, Changsha, China, in 2004, the M.S. degree in control theory and control engineering from the Guangdong University of Technology, Guangzhou, China, in 2009, and the Ph.D. degree in electrical engineering from the South China University of Technology, Guangzhou, in 2015. Since September 2014, he has been a Lecturer with the Department of Electrical Engineering, Dongguan University of Technology, Dongguan, China. His research interests include control theories and motor drives.

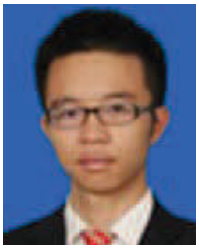

BIHUA HU received the B.S. degree in automation and the M.S. degree in power engineering from Xiangtan University, Xiangtan, China, in 2011 and 2014, respectively, and the Ph.D. degree in power electronics and power drives from the South China University of Technology, Guangzhou, China, in 2019.

Since August 2019, he has been a Lecturer with the School of Automation and Electronic Information, Xiangtan University. His current research interests include energy storage, multilevel converters, and the application of power electronics in renewable energy systems.

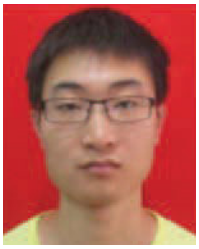

WANG HU was born in Hunan, China, in 1992. He received the B.S. degree in electronic engineering from the University of South China, Hengyang, China, in 2015, and the M.S. degree in electrical engineering from the Guangdong University of Technology, Guangzhou, China, in 2018. He is currently pursuing the Ph.D. degree in power electronic with the School of Electric Power, South China University of Technology, Guangzhou.

His current research interests include high-power density rectifiers, matrix converters, and nonlinear control strategies.